

## Studies of visible-light-driven Sm-doped ZnO nanoparticles synthesized by combustion method

A. Phuruangrat<sup>a,\*</sup>, S. Thamsukho<sup>a</sup>, S. Thungprasert<sup>b</sup>, T. Sakhon<sup>c</sup>,  
T. Thongtem<sup>d,e</sup>, S. Thongtem<sup>d,f</sup>

<sup>a</sup>*Department of Materials Science and Technology, Faculty of Science,  
Prince of Songkla University, Hat Yai, Songkhla 90112, Thailand*

<sup>b</sup>*Department of Chemistry and Applied Chemistry, Faculty of Science,  
Lampang Rajabhat University, Lampang 52100, Thailand*

<sup>c</sup>*Electron Microscopy Research and Service Center, Faculty of Science,  
Chiang Mai University, Chiang Mai, 50200, Thailand*

<sup>d</sup>*Materials Science Research Center, Faculty of Science,  
Chiang Mai University, Chiang Mai 50200, Thailand*

<sup>e</sup>*Department of Chemistry, Faculty of Science, Chiang Mai University,  
Chiang Mai 50200, Thailand*

<sup>f</sup>*Department of Physics and Materials Science, Faculty of Science,  
Chiang Mai University, Chiang Mai 50200, Thailand*

ZnO nanoparticles with different Sm doping contents were prepared by tartaric acid solution combustion method and followed by calcination at 600 °C for 2 h. The XRD patterns of ZnO and Sm-doped ZnO samples were indexed to the pure phase of hexagonal wurtzite ZnO structure. TEM images of ZnO and Sm-doped ZnO samples show that the samples contained nanoparticles with different particle sizes. Their particle sizes were decreased with increasing in the weight contents of Sm dopant. Their photocatalytic properties were also investigated through the photodegradation of methylene blue (MB) under visible light irradiation. The 3% Sm-doped ZnO nanoparticles have the highest photodegradation of MB under visible light irradiation because Sm<sup>3+</sup> as an electron acceptor played the role in inhibiting the recombination of charge carrier pairs and enhancing the photocatalytic performance of ZnO under visible light irradiation.

(Received December 29, 2021; Accepted March 11, 2022)

**Keywords:** Sm-doped ZnO, Nanoparticles, Photocatalysis, Combustion method

### 1. Introduction

In recent years, the advanced oxidation processes (AOPs) have been widely used in degradation of organic pollutants by production of highly reactive hydroxyl radicals under light irradiation which is higher performance than tradition water treatment method because organic compound completely mineralizes into H<sub>2</sub>O and CO<sub>2</sub> without causing secondary pollutions [1-4]. Zinc oxide (ZnO) with high exciton binding energy of 60 meV and wide band gap (3.37 eV) is a promising semiconductor photocatalyst which has been widely used in various fields, including antibacterial agents, solar cells, light-emitting diodes, nano-lasers, piezoelectric devices, UV-shielding materials and gas sensors because of its low toxicity, high oxidative capacity, high physical and chemical stability, long-life span and low cost [1, 3, 5-7]. Nevertheless, the charge carrier recombination and absorption in only ultraviolet light of ZnO are relatively high and seriously restrict its practical applications in photocatalytic process [1, 3, 7, 8]. To tackle this challenge, rare earth such as Gd [8, 9], Ce [10, 11], Er [12], Eu [13, 14, 15], Y [16, 17] and Pr [18] doped in ZnO matrix is a promising method for reducing its band gap, improving charge carrier separation, inhibiting the recombination of photocarriers and changing the threshold wavelength of the absorbed light to the visible region [1, 2, 7, 8]. The chemical routes such as hydrothermal [1,

---

\* Corresponding author: phuruangrat@hotmail.com  
<https://doi.org/10.15251/JOR.2022.182.149>

7, 15], co-precipitation [6, 9, 10, 11], combustion [8, 19-23], sol-gel [12, 16, 18] and microwave-assisted solution method [17, 24] have been reported for synthesizing of ZnO nanoparticles. Among them, combustion method has attracted much attention due to the highly crystalline materials, high purity, high specific surface area, large scale synthesis and low temperature synthesis [8, 19-23]

In the present work, the Sm-doped ZnO nanoparticles were synthesized by combustion method using tartaric acid as a fuel and followed by high temperature calcination. Phase, morphology, oxidation state of element and photocatalytic activity were studied. The photocatalytic properties of Sm-doped ZnO nanoparticles were investigated through photodegradation of methylene blue (MB) under visible light irradiation.

## 2. Experimental procedure

All the chemicals used in the present study were analytical grade and used without further purification. Zinc nitrate hexahydrate ( $\text{Zn}(\text{NO}_3)_2 \cdot 6\text{H}_2\text{O}$ ), 95% ethanol ( $\text{C}_2\text{H}_5\text{OH}$ ) and samarium (III) nitrate hexahydrate ( $\text{Sm}(\text{NO}_3)_3 \cdot 6\text{H}_2\text{O}$ ) were purchased from Sigma-Aldrich Corporation, UK. Tartaric acid ( $\text{C}_4\text{H}_6\text{O}_6$ ) and methylene blue ( $\text{C}_{16}\text{H}_{18}\text{ClN}_3\text{S}$ ) were purchased from Loba Chemie PVT. Ltd., India. Sodium hydroxide (NaOH) was purchased from RCI Labscan Ltd., Thailand.

Each 0.01 mol  $\text{Zn}(\text{NO}_3)_2 \cdot 6\text{H}_2\text{O}$  and 0–5%  $\text{Sm}(\text{NO}_3)_3 \cdot 6\text{H}_2\text{O}$  by weight were weighed and dissolved in 50 ml  $\text{C}_2\text{H}_5\text{OH}$  solutions under continued stirring. Subsequently, 0.01 mol tartaric acid in 50 ml  $\text{C}_2\text{H}_5\text{OH}$  solution was added to these solutions to form gel precursors. Then, 1 M 20 ml NaOH solution in  $\text{C}_2\text{H}_5\text{OH}$  solution was also added to them with continued stirring for 30 min. The as-synthesized gel precursors were filtered, washed with distilled water, dried and further calcined in air at 600 °C for 2 h.

Thermal analysis of dried gel was analyzed by thermogravimetric analysis (TGA 8000 Simultaneous Thermal Analyzer (STA Perkin Elmer) in nitrogen atmosphere with 10 °C.min<sup>-1</sup> heating rate at T<sub>R</sub>–800 °C. X-ray diffraction (XRD) operated by a Philips X'Pert MPD X-ray diffractometer with Cu K<sub>α</sub> radiation in the 2θ range of 10–80 deg with a scanning rate of 0.02 deg.s<sup>-1</sup>. The morphologies were characterized by transmission electron microscopy (TEM) and selected area electron diffraction (SAED) using a JEOL JEM-2010 TEM operating at 200 kV. X-ray photoelectron spectroscopy (XPS) was carried out using an Axis Ultra DLD | Kratos–Kratos Analytical with a monochromated Al K<sub>α</sub> radiation (1486.6 eV) as a providing source. All the XPS spectra were calibrated relative to the C 1s electron peak at 285.0 eV.

The photocatalytic activities of the as-synthesized samples were determined by measuring the degradation of methylene blue (MB) solutions under visible light irradiation from a xenon lamp. Each 200 mg of the photocatalysts was added in 200 ml 10<sup>-5</sup> M MB aqueous solutions. Prior to the test, the suspensions were magnetically stirred in the dark for 30 min to establish an adsorption/desorption equilibrium of MB on surfaces of the photocatalysts. During photocatalytic test, 5 ml solution was withdrawn at a period of time and centrifuged to remove the photocatalytic solid. The concentration of MB solution was analyzed by a Perkin Elmer Lambda 25 UV-visible spectrometer at 664 nm wavelength. The decolorization efficiency was calculated by the following equation.

$$\text{Decolorization efficiency (\%)} = \frac{C_o - C_t}{C_o} \times 100 \quad (1)$$

, where C<sub>o</sub> is the initial concentration of MB and C<sub>t</sub> is the concentration of MB after UV light illumination within the elapsed time (t).

## 3. Results and discussion

The thermal behavior of dried precursor was investigated by thermogravimetric analysis (TGA) at  $T_R=800$  °C with heating rate of  $10$  °C.min<sup>-1</sup> in nitrogen atmosphere and shown in Fig. 1. The TGA graph of dried precursor shows two steps of weight losses which are assigned to the dehydration of absorbed moisture at  $T_R=250$  °C and burning the tartaric acid and volatile group such as nitride at  $250-600$  °C [20, 21, 25, 26]. No significant weight loss at a temperature higher than  $600$  °C, implying the suitable calcination of dried precursors at  $600$  °C.

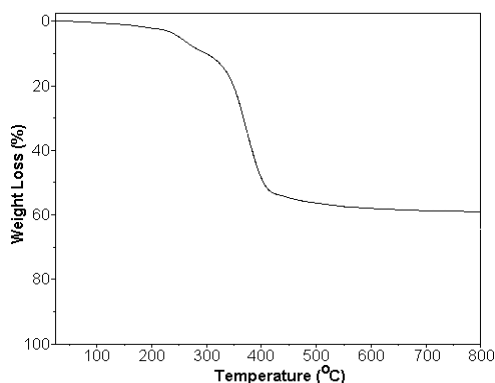


Fig. 1. TGA graph of Zn-tartaric acid precursor with 5% Sm dopant at  $T_R=800$  °C in nitrogen atmosphere.

XRD of all synthesized Sm-doped ZnO samples were carried out to confirm the formation of ZnO with different weight contents of Sm dopant. Fig. 2 shows the XRD patterns of Sm-doped ZnO with different weight contents of Sm dopant in  $2\theta = 10^\circ-80^\circ$  with a scanning rate of  $0.02$  deg.s<sup>-1</sup>. Pure ZnO sample without Sm dopant can be indexed to the hexagonal wurtzite ZnO structure of the JCPDS No. 36-1451 [27].

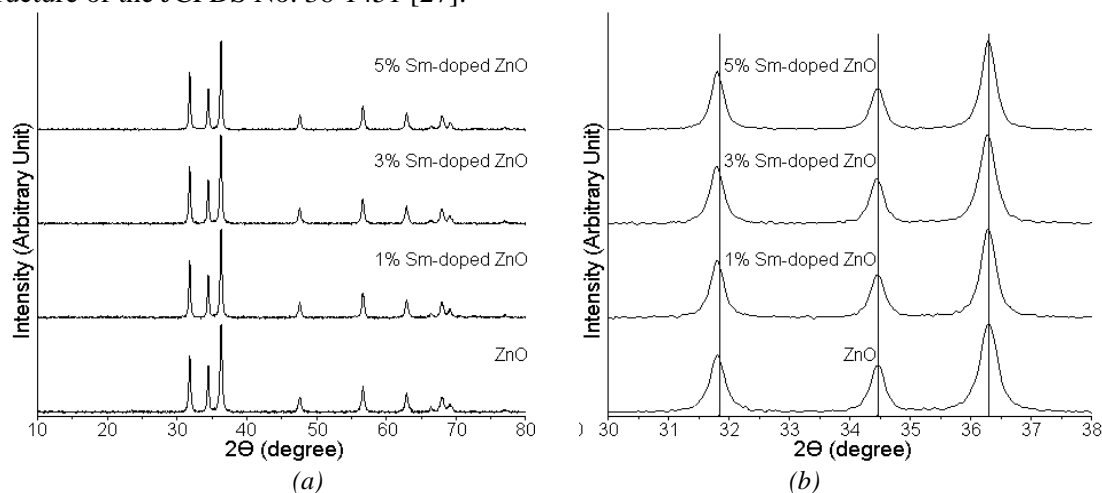


Fig. 2. XRD patterns of 0–5% Sm-doped ZnO samples synthesized by a tartaric acid combustion method over the  $2\theta$  range of (a)  $10^\circ-80^\circ$  and (b)  $30^\circ-38^\circ$ .

When ZnO was doped with Sm, the Sm dopant did not have the influence to change the XRD patterns of Sm-doped ZnO, indicating that the structure of Sm-doped ZnO samples were still the pure phase of hexagonal wurtzite ZnO structure. The impurity peaks such as  $\text{Sm}(\text{OH})_3$ ,  $\text{Sm}_2\text{O}_3$  and  $\text{Zn}(\text{OH})_2$  were not detected in XRD patterns of Sm-doped ZnO samples, indicating that the  $\text{Sm}^{3+}$  ions were incorporated in ZnO lattice. Moreover, the main diffraction peaks of XRD patterns of Sm-doped ZnO samples at  $2\theta$  of  $30^\circ-38^\circ$  were shifted towards lower angle comparing to the pure ZnO sample because the larger  $\text{Sm}^{3+}$  ion ( $0.96$  Å [28-30]) substituted for the smaller  $\text{Zn}^{2+}$  ion

(0.74 Å [8, 11, 12, 15, 18]) of ZnO lattice. The average particle sizes of all samples were calculated by Scherrer equation.

$$D = 0.9\lambda/\beta\cos\theta \quad (2)$$

, where  $D$  is the average crystallite size,  $\lambda$  is the wavelength of Cu  $K_{\alpha}$  (0.154046 nm),  $\beta$  is the full width at half maximum (FWHM) of the diffraction peak and  $\theta$  is Bragg's angle [1, 8, 9, 11]. The average particle sizes of samples were 89.32 nm, 84.40 nm, 72.96 nm and 66.93 nm for 0%, 1%, 3% and 5% Sm-doped ZnO nanostructure, respectively. The average particle size of Sm-doped ZnO sample was decreased with increasing in the weight content of Sm dopant due to the distortion of ZnO host lattice caused by the addition of  $\text{Sm}^{3+}$  ions which can lead to reduce the nucleation and grain growth rates of Sm doped ZnO nanoparticles [1, 8, 9, 11, 31].

The chemical composition and oxidation state of 3% Sm-doped ZnO sample were analyzed by XPS using carbon C 1s peak at 285.0 eV as a calibration standard. The presence of Sm, Zn and O in 3% Sm-doped ZnO sample was detected in the full survey XPS spectrum at 0-1200 eV (Fig. 3a).

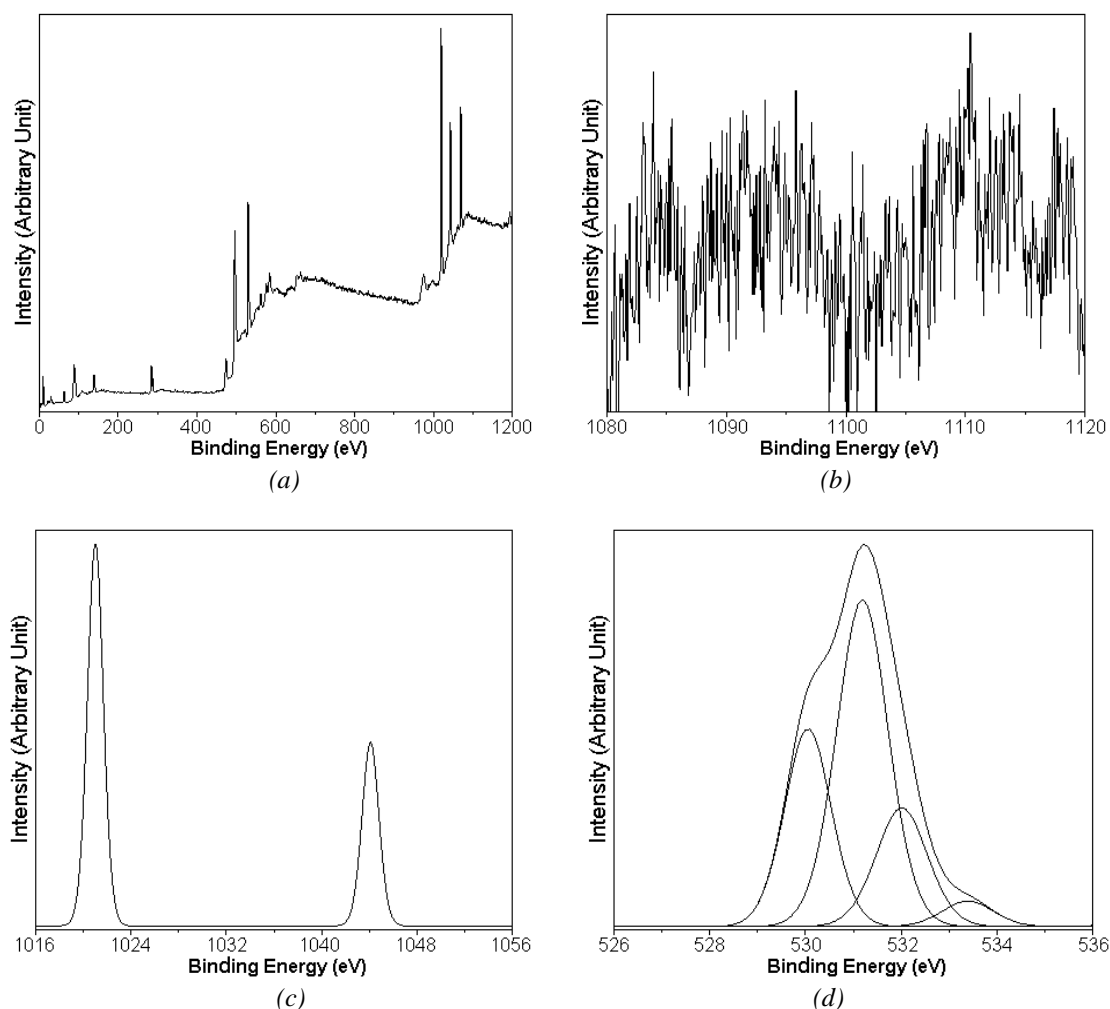


Fig. 3 (a) XPS survey spectrum and high-resolution XPS spectra of (b) Sm 3d, (c) Zn 2p and (d) O 1s of 3% Sm-doped ZnO sample.

The high-resolution binding energy XPS spectra of Sm 3d, Zn 2p and O 1s core levels of 3% Sm-doped ZnO sample are shown in Fig. 3b-d. The high-resolution binding energies of Sm 3d

core level of 3% Sm-doped ZnO sample locate at 1082.9 eV for Sm  $3d_{5/2}$  and 1110.39 eV for Sm  $3d_{3/2}$  which are assigned to the oxidation state of  $\text{Sm}^{3+}$  ions, confirming that the  $\text{Sm}^{3+}$  ions substituted for  $\text{Zn}^{2+}$  ions in ZnO lattice [32-34]. The XPS spectra of Zn 2p core level shows the two binding energies centered at 1021.02 eV and 1044.12 eV for 3% Sm-doped ZnO which are associated to the Zn  $2p_{3/2}$  and Zn  $2p_{1/2}$  core levels, respectively [7-9, 11, 18]. The energy difference of 2p core level is about 23.10 eV indicating that Zn species in 3% Sm-doped ZnO sample is  $\text{Zn}^{2+}$  ion [7-9, 11, 18]. The asymmetric high resolution binding energy of O 1s core level of 3% Sm-doped ZnO sample was fitted by the Gaussian analysis. They show the symmetric high resolution binding energies of O 1s at 530.06, 531.19, 532.01 and 533.39 eV for 3% Sm-doped ZnO which are related to the lattice oxygen containing in Zn lattice, oxygen deficient region and chemisorbed oxygen ions such as  $\text{H}_2\text{O}$  and  $\text{CO}_2$ , respectively [7-9, 11, 18]. The strength of binding energy of oxygen deficient region of Sm-doped ZnO is the highest because the Sm dopant can play the role in increasing oxygen vacancy of ZnO lattice and enhancing the photocatalytic reaction of ZnO [11, 18, 32].

Fig. 4 shows the TEM images and SAED patterns of ZnO with and without Sm dopant. The TEM image of ZnO without Sm dopant shows the homogenous distribution of nanoparticles with 50-200 nm range. Moreover, the particle size of Sm-doped ZnO samples were decreased with the increase of weight content of Sm dopant in accordance with the Scherrer calculation. The particle sizes of samples were  $88.10 \pm 23.99$  nm,  $25.84 \pm 3.55$  nm,  $24.46 \pm 7.41$  nm and  $24.33 \pm 7.72$  nm for 0%, 1%, 3% and 5% Sm-doped ZnO nanoparticles, respectively. The Sm-doped ZnO samples were composed of spherical nanoparticles with agglomeration increasing of particles due to the decrease of surface energy of nanoparticles. The typical selected area of electron diffraction (SAED) patterns of the ZnO and Sm-doped ZnO nanoparticles show the bright continuous spots of electron diffraction pattern which certified the highly crystalline nature of ZnO. The typical electron diffraction rings of ZnO with and without Sm doped nanoparticles correspond to the (100), (002), (101), (102), (110), (103), (112) and (201) planes of hexagonal wurtzite ZnO structure of the JCPDS No. 36-1451.

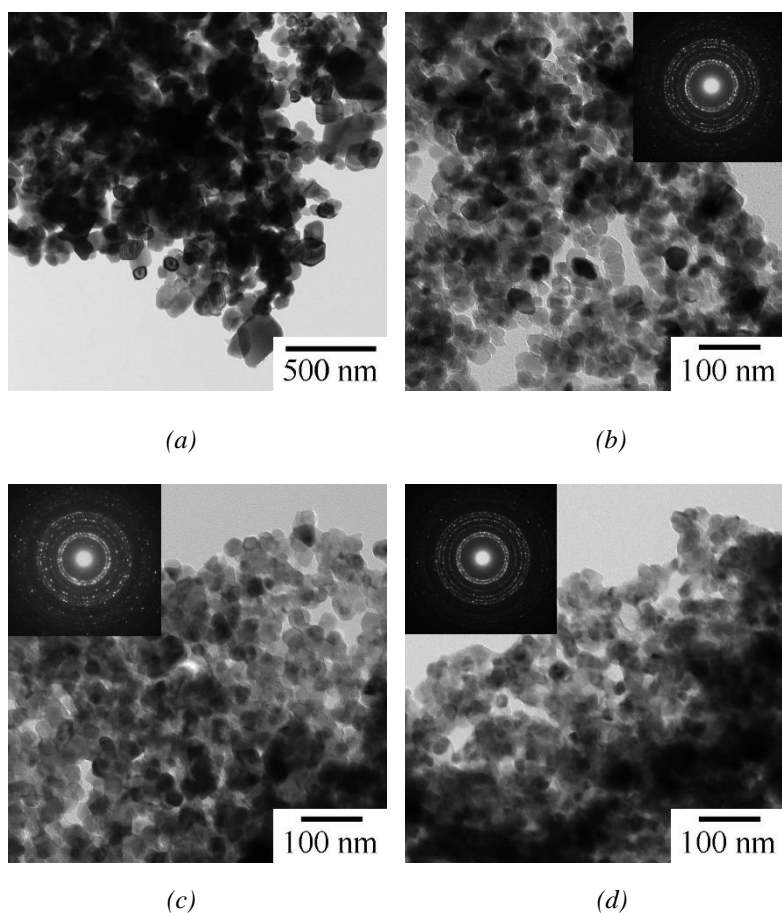


Fig. 4. TEM images and SAED patterns of (a) 0%, (b) 1%, (c) 3% and (d) 5% Sm-doped ZnO samples synthesized by a tartaric acid-assisted precipitation method.

Fig. 5a shows the photodegradation of MB over the ZnO samples with and without Sm dopant under visible radiation. The pure ZnO nanoparticles show low photodegradation efficiency of MB of 21.16% under visible light irradiation within 100 min. They can be seen that the photodegradation efficiencies of the samples were increased with increasing in the weight of Sm dopant to 3%. The photodegradation efficiency of 3% Sm-doped ZnO nanoparticles under visible light irradiation was increased to 96.78%. For more than 3% Sm dopant, the photodegradation efficiency of 5% Sm-doped ZnO nanoparticles under visible light irradiation was slightly decreased to 91.67%. They can be concluded that Sm dopant played the role in improving the effective charge carrier separation because  $\text{Sm}^{3+}$  played the role in accepting the photo-excited electron from conduction band of ZnO and  $\text{Sm}^{2+}$  formed. Thus, the rate of recombination of charge carriers was reduced and the photocatalytic performance of ZnO under visible light irradiation was increased [8, 9, 11, 14]. The photodegradation efficiency of ZnO with and without Sm dopant under visible light was fitted through the pseudo-first-order kinetics shown in Fig. 5b [4, 8, 11, 16]. They show the linear lines of the plotted graphs of the  $\ln(C_0/C_t)$  versus irradiation time, indicating that all MB degradation efficiencies over all photocatalysts are pseudo-first-order kinetics model [4, 8, 11, 16]. The calculated rate constants of MB degradation over all photocatalysts were  $2.19 \times 10^{-3}$ , 0.0163, 0.0325 and  $0.0234 \text{ min}^{-1}$  for 0%, 1%, 3% and 5% Sm-doped ZnO nanoparticles. The 3% Sm-doped ZnO nanoparticles have the highest degradation kinetics for MB under visible light irradiation which is 15 times that of ZnO nanoparticles.

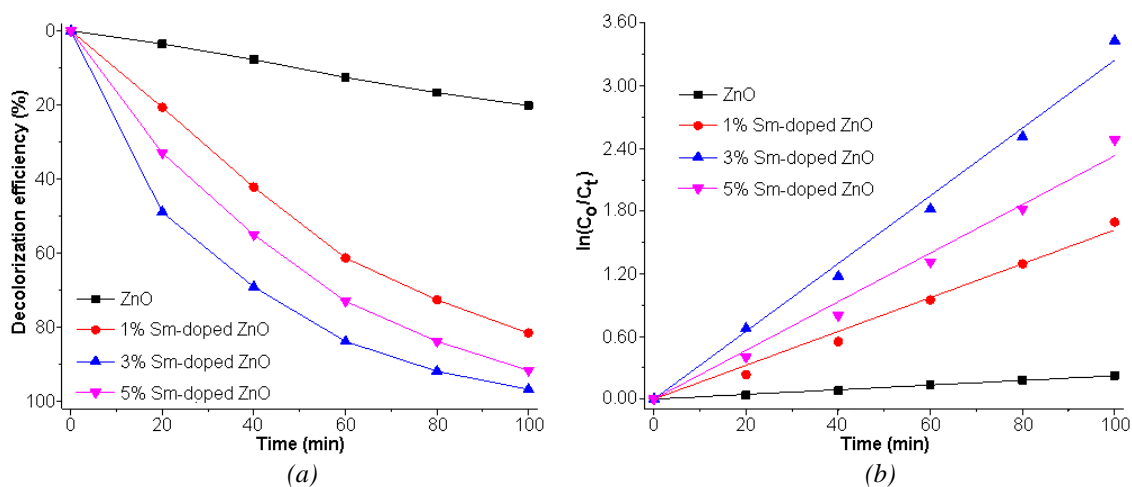


Fig. 5 (a) Decolorization efficiency and (b) reaction kinetics for the degradation of MB molecules photocatalyzed by 0–5% Sm-doped ZnO samples illuminated by visible radiation.

The photocatalytic mechanism of Sm-doped ZnO nanoparticles under visible radiation is shown in Fig. 6. When visible light irradiated on the surface of Sm-doped ZnO nanoparticles, electrons ( $e^-$ ) were excited from the valence band (VB) to the conduction band (CB) and holes ( $h^+$ ) were induced in VB of Sm-doped ZnO nanoparticles [1, 6, 8, 9, 11]. Then, the photo-excited electrons reacted with the adsorbed oxygen on the surface of Sm-doped ZnO nanoparticles to form superoxide anions ( $\bullet\text{O}_2^-$ ) while the photo-induced holes reacted with the surface-bonded  $\text{H}_2\text{O}$  or  $\text{OH}^-$  on the surface of Sm-doped ZnO nanoparticles to form hydroxyl radicals ( $\bullet\text{OH}$ ) [1, 6, 8, 9, 11]. The reactive species directly oxidized and transformed the dye molecules into  $\text{CO}_2$  and  $\text{H}_2\text{O}$  [1, 6, 8, 9, 11]. The  $\text{Sm}^{3+}$  ions as electron accepters played the role in preventing the electron–hole recombination and enhancing the photocatalytic reaction [8, 9, 11, 35]. Thus, the active species such as  $\bullet\text{O}_2^-$ ,  $\bullet\text{OH}$  and  $h^+$  were determined for MB degradation over Sm-doped ZnO nanoparticles.

To investigate the active species, ethylenediaminetetraacetic acid disodium salt (EDTA-2Na), isopropyl alcohol (IPA) and benzoquinone (BQ) were added to the reactant solutions as the active scavengers of  $h^+$ ,  $\cdot OH$  and  $\cdot O_2^-$ , respectively [1, 5, 36, 37]. Fig. 7 shows the effect of different scavengers on the degradation of MB photocatalyzed by 3% Sm-doped ZnO nanoparticles under visible light irradiation. In this research, the MB degradation efficiency was decreased to 75.68%, 8.32% and 19.75% for EDTA-2Na, IPA and BQ adding, respectively. In conclusion, the formation of  $\cdot OH$  radicals played a major role in the photocatalytic degradation of MB over 3% Sm-doped ZnO nanoparticles under visible light irradiation.

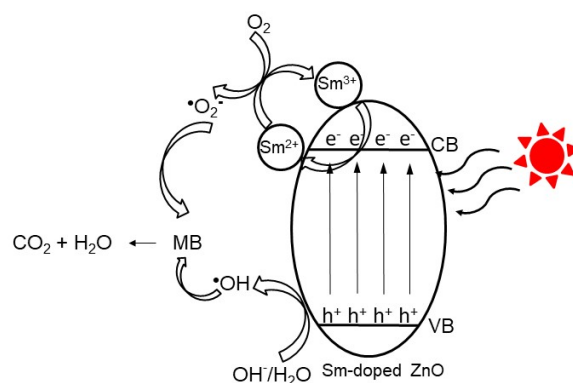


Fig. 6. The photocatalytic mechanism of MB molecules photocatalyzed by Sm-doped ZnO sample illuminated by visible radiation.

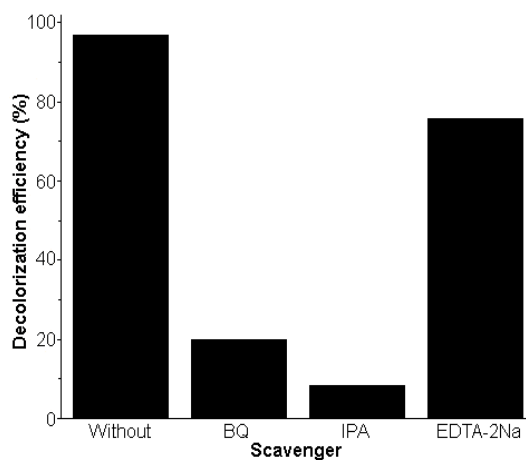
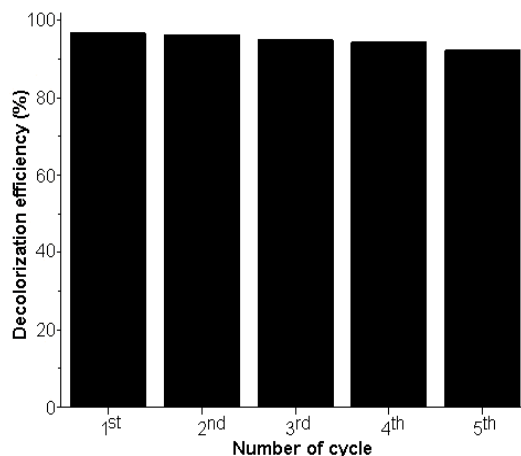


Fig. 7. Effect of different scavengers on the degradation of MB photocatalyzed by 3% Sm-doped ZnO nanoparticles under visible light irradiation.



*Fig. 8. Stability and recyclability of the reused 3% Sm-doped ZnO nanoparticles illuminated by visible light within five cycles.*

Fig. 8 shows the photocatalytic degradation of MB in the presence reused Sm-doped ZnO nanoparticles under visible light irradiation. At the end of the 5<sup>th</sup> cycle, the photodegradation efficiency of reused Sm-doped ZnO nanoparticles was decreased to 92.31%. Thus, the Sm-doped ZnO nanoparticles are the excellent reusability and long-term stability for photodegradation of dye under visible light irradiation.

#### 4. Conclusions

ZnO nanoparticles with different weight contents of Sm dopant were synthesized by tartaric acid combustion method and followed by calcination at 600 °C for 2 h. In this research, all the as-synthesized products were pure hexagonal wurtzite ZnO nanoparticles with size of  $88.10 \pm 23.99$  nm,  $25.84 \pm 3.55$  nm,  $24.46 \pm 7.41$  nm and  $24.33 \pm 7.72$  nm for 0%, 1%, 3% and 5% Sm-doped ZnO nanoparticles, respectively. The 3% Sm-doped ZnO nanoparticles show the highest photodegradation of MB under visible light irradiation which is 15 times that of ZnO nanoparticles because Sm<sup>3+</sup> as an electron acceptor played the role in inhibiting the recombination of charge carrier pairs and enhancing the photocatalytic performance of ZnO under visible light irradiation. The product shows the excellent reusability and long-term stability for photodegradation of the dye under visible light irradiation.

#### Acknowledgement

The research was supported by the contract number SCI6402026S, Prince of Songkla University, Thailand.

#### References

- [1] Z. Mirzaeifard, Z. Shariatinia, M. Jourshabani, S.M.R. Darvishi, *Ind. Eng. Chem. Res.* 59, 15894 (2020); <https://doi.org/10.1021/acs.iecr.0c03192>
- [2] Y. Song, Z. Sun, Y. Wu, Z. Chai, X. Wang, *Inorg. Chem.* 57, 8558 (2018); <https://doi.org/10.1021/acs.inorgchem.8b01287>
- [3] V.N. Nguyen, D.T. Tran, M.T. Nguyen, T.T.T. Le, M.N. Ha, M.V. Nguyen, T.D. Pham, *Res. Chem. Intermed.* 44, 3081 (2018); <https://doi.org/10.1007/s11164-018-3294-3>
- [4] A. Saffar-Teluri, S. Bolouk, M.H. Amini, *Res. Chem. Intermed.* 39, 3345 (2013); <https://doi.org/10.1007/s11164-012-0847-8>

- [5] A.İ. Vaizoğullar, *Res. Chem. Intermed.* 47, 2701 (2021); <https://doi.org/10.1007/s11164-021-04438-2>
- [6] F. Xu, D. Guo, H. Han, H. Wang, Z. Gao, D. Wu, K. Jiang, *Res. Chem. Intermed.* 38, 1579 (2012); <https://doi.org/10.1007/s11164-012-0485-1>
- [7] J. Wang, X. H. Sun, H. Du, *Russ. J. Inorg. Chem.* 65, 1111 (2020); <https://doi.org/10.1134/S0036023620070244>
- [8] S. Sa-nguanprang, A. Phuruangrat, T. Thongtem, S. Thongtem, *Russ. J. Inorg. Chem.* 64, 1600 (2019); <https://doi.org/10.1134/S0036023619120143>
- [9] S. Selvaraj, M.K. Mohan, M. Navaneethan, S. Ponnusamy, C. Muthamizhchelvan, *Mater. Sci. Semicond. Process.* 103, 104622 (2019); <https://doi.org/10.1016/j.mssp.2019.104622>
- [10] H.F. Moafi, M. Hafezi, S. Khorram, M.A. Zanjanchi, *Plasma Chem. Plasma Process.* 37, 159 (2017); <https://doi.org/10.1007/s11090-016-9748-8>
- [11] G. Vijayaprasath, P. Soundarrajan, G. Ravi, *J. Electron. Mater.* 48, 684 (2019); <https://doi.org/10.1007/s11664-018-6763-y>
- [12] S. Bhatia, N. Verma, *J. Mater. Sci.* 29, 14960 (2018); <https://doi.org/10.1007/s10854-018-9634-7>
- [13] P. Franco, O. Sacco, I.D. Marco, D. Sannino, V. Vaiano, *Top. Catal.* 63, 1193 (2020); <https://doi.org/10.1007/s11244-020-01279-y>
- [14] Y. Zong, Z. Li, X. Wang, J. Ma, Y. Men, *Ceram. Inter.* 40, 10375 (2014); <https://doi.org/10.1016/j.ceramint.2014.02.123>
- [15] L. Luo, L. Zhu, X. Wang, *Appl. Mech. Mater.* 700, 482 (2015); <https://doi.org/10.4028/www.scientific.net/AMM.700.482>
- [16] H. Parangusan, D. Ponnamma, M.A.A. Al-Maadeed, A. Marimuthu, *Photochem. Photobiol.* 94, 237 (2018); <https://doi.org/10.1111/php.12867>
- [17] P.K. Sanoop, S. Anas, S. Ananthakumar, V. Gunasekar, R. Saravanan, V. Ponnusami, *Arab. J. Chem.* 9, S1618 (2016); <https://doi.org/10.1016/j.arabj.2012.04.023>
- [18] I. Ahmad, M.S. Akhtar, E. Ahmed, M. Ahmad, *J. Mater. Sci.* 31, 1084 (2020); <https://doi.org/10.1007/s10854-019-02620-2>
- [19] A.C. Lucilha, R. Afonso, P.R.C. Silva, L.F. Lepre, R.A. Ando, L.H. Dall'Antonia, *J. Braz. Chem. Soc.* 25, 1091 (2014)
- [20] H.V. Vasei, S.M. Masoudpanah, M. Adeli, M.R. Aboutalebi, *J. Sol-Gel Sci Technol.* 89, 586 (2019); <https://doi.org/10.1007/s10971-018-4900-y>
- [21] Z.K. Bolaghi, M. Hasheminasari, S.M. Masoudpanah, *Ceram Inter.* 44, 12684 (2018); <https://doi.org/10.1016/j.ceramint.2018.04.069>
- [22] N. Riahi-Noori, R. Sarraf-Mamoory, P. Alizadeh, A. Mehdikhani, *J. Ceram. Process. Res.* 9, 246 (2008)
- [23] X. Kang, C. Li, Z. Zheng, X. Cui, *Combust. Sci. Technol.* 193, 75 (2021); <https://doi.org/10.1080/00102202.2019.1650270>
- [24] M. Hasanpoor, M. Aliofkhazraei, H. Delavari, *Procedia Mater. Sci.* 11, 320 (2015) 320-325; <https://doi.org/10.1016/j.mspro.2015.11.101>
- [25] S.K. Chawla, P. Kaur, R.K. Mudsainiyan, S.S. Meena, S.M. Yusuf, *J. Supercond. Nov. Magn.* 28, 1589 (2015); <https://doi.org/10.1007/s10948-014-2893-5>
- [26] K. Duangsa, A. Tangtrakarn, C. Mongkolkachit, P. Aungkavattana, K. Moolsarn, *Adv. Mater. Sci. Eng.* 2021, 5592437 (2021); <https://doi.org/10.1155/2021/5592437>
- [27] Powder Diffract. File, JCPDS Internat. Centre Diffract. Data, PA 19073–3273, U.S.A. (2001).
- [28] J. Divya, N.J. Shivaramu, W.D. Roos, W. Purcell, H.C. Swart, *J. Alloy. Compd.* 854, 157221 (2021); <https://doi.org/10.1016/j.jallcom.2020.157221>
- [29] Z. Xiaw, D. Chen, *J. Am. Ceram. Soc.* 93, 1397 (2010)
- [30] Y. Alajlani, M. Oglakci, U.H. Kaynar, M. Ayvaciikli, Z.G. Portakal-Uçar, M. Topaksu, N. Can, *J. Asian Ceram. Soc.* 9, 291 (2021); <https://doi.org/10.1080/21870764.2020.1864898>
- [31] L. Anju Chanu, W.J. Singh, K.J. Singh, K. Nomita Devi, *Results Phys.* 12, 1230 (2019); <https://doi.org/10.1016/j.rinp.2018.12.089>
- [32] D. Ranjith Kumar, K.S. Ranjith, R.T. Rajendra Kumar, *Optik* 154, 115 (2018); <https://doi.org/10.1016/j.ijleo.2017.10.004>

- [33] H. Yu, J. Xu, H. Guo, Y. Li, Z. Liu, Z. Jin, RSC Adv. 7, 56417 (2017); <https://doi.org/10.1039/C7RA11849J>
- [34] D. Narsimulu, B.N. Rao, G. Nagaraju, J.S. Yu, N. Satyanarayana, Journal of Solid State Electrochemistry 24, 225 (2020); <https://doi.org/10.1007/s10008-019-04484-2>
- [35] H. Parangusan, D. Ponnamma, M.A.A. Al-Maadeed, A. Marimuthu, Photochemistry and Photobiology 94, 237 (2018); <https://doi.org/10.1111/php.12867>
- [36] J. Du, J. Zhang, T. Yang, R. Liu, Z. Li, D. Wang, T. Zhou, Y. Liu, C. Liu, G. Che, Catalysts 11, 24 (2021); <https://doi.org/10.3390/catal11010024>
- [37] Z. Jiao, Z. Liu, Z. Ma, ACS Omega 4, 7919 (2019); <https://doi.org/10.1021/acsomega.9b00806>